ELSEVIER

Journal of Nuclear Materials 299 (2001) 111–123

journal of nuclear materials

www.elsevier.com/locate/jnucmat

Effect of the expansion associated with the plutonium α–β–γ phase transitions on storage can integrity

Dane R. Spearing [a,*], D. Kirk Veirs [a], F. Coyne Prenger [b]

[a] Los Alamos National Laboratory, Nuclear Materials Technology Division, MS E505, Los Alamos, NM 87545, USA
[b] Los Alamos National Laboratory, Engineering Sciences and Applications Division, Los Alamos, NM 87545, USA

Received 3 April 2001; accepted 15 August 2001

Abstract

The effects of the volume expansion of plutonium metal through the α–β and β–γ phase transitions on a stainless steel storage container were examined. A cylindrical plutonium ingot was placed in the axial center of an annealed stainless steel cylinder and thermally cycled until a steady state in the strain response of the cylinder was reached. The average plastic hoop strain was 1.47% and 1.55% after six and four cycles through the α–β and α–β–γ phase transitions, respectively. Elastic strain was ~0.2%, indicating a 8.96 MPa back pressure on the Pu ingot. This is an order of magnitude less than the compressive yield strength of α- and β-Pu at the transition temperature. Metallographic analyses indicate that anisotropic expansion of the Pu ingot is due to preferentially oriented grain growth of the β-Pu along the axial direction due to stress applied by the steel cylinder during the α–β phase transition. Published by Elsevier Science B.V.

1. Introduction

The previous US Department of Energy (DOE) standard for the stabilization, packaging, and storage of plutonium bearing materials [1] specified a maximum temperature of 100 °C for the storage of alpha-phase Pu metal (α-Pu). The rationale for this maximum temperature was to prevent the possibility of compromising the integrity of the standard-specified stainless steel storage cans due to the large volume expansions associated with the plutonium alpha to beta (~10 vol.%) and the beta to gamma (~3 vol.%) phase transitions, which occur at 120 °C and ~200 °C, respectively. The assumption was that pieces of α-Pu metal tightly fit within the container had the potential for deforming the wall of a storage container beyond accepted criteria [2] upon transforming to β-Pu and/or via repeated cycling through the α–β transition. Within current proposed storage facilities (such as the Actinide Storage Facility at the DOE Savannah river site (SRS)), credible scenarios exist in which local temperatures could significantly exceed the Pu α–β transition temperature, and could get as high as the β–γ transition temperature. The purpose of this study was to experimentally determine the effects of the volume expansion of the α–β and α–β–γ transformations of plutonium metal on a stainless steel storage container of the type specified by the plutonium storage standard. In addition, the effects of the radial compression imposed by the storage cylinder on the bulk properties and microstructure of the plutonium metal were examined. The results from these experiments support the technical basis for the revised DOE storage standard [3] that allows for storage of unalloyed Pu above 100 °C.

2. Literature review

A number of studies have been published on the effects of a variety of variables (e.g., pressure,

* Corresponding author. Tel.: +1-505 665 1465; fax: +1-505 665 4394.
E-mail address: dane@lanl.gov (D.R. Spearing).

0022-3115/01/$ - see front matter. Published by Elsevier Science B.V.
PII: S0022-3115(01)00683-3

deformation, grain size) relevant to the Pu α–β phase transition, which can be used to make qualitative predictions as to how the Pu and storage container will interact though the course of thermal cycling through the phase transition. The mechanism of the α–β phase transition is still not well understood, although several studies suggest that it is martensitic in nature [4,5]. The α to β and β to α transformation kinetics have been extensively studied, and show that the transformations exhibit simple time–temperature–transformation (T–T–T) curves with significant hysteresis [5,6]. The effects of deformation and stress on the kinetics of the phase transition have also been examined [5,6], and it was found that plastic deformation of the α-phase accelerates the α to β transformation, with the acceleration attributable only to residual stresses. It was also found that plastic deformation of the β-phase retards kinetics of the back transformation from β to α. Thus, plastic deformation tends to stabilize the higher temperature β-phase. Conversely, applied uniaxial compressive stress raises the starting temperatures for both the α to β and β to α transformations, while tensile stress lowered the α to β starting temperature [5]. This is consistent with the experimentally determined P–T phase diagram for pure plutonium [7], in which the α-phase is stabilized by increasing isostatic pressure.

The effect of applied stress on grain orientation and grain growth has been studied, and it was found that α-Pu displays a preferential growth in specific crystallographic directions as a function of the applied distribution of elastic stresses during the β to α phase transition [8]. Further study determined that α-Pu will form columnar grains with the (020) planes aligned perpendicular to the applied compressive stress direction [9], forming the well-known 'veining phenomenon'. This technique has been used to grow oriented specimens of Pu for electrical resistivity studies [10]. Interestingly, in the absence of any applied stresses, both the α to β and β to α transformation volume changes occur anisotropically [5]. Based on this observation, it was concluded that these anisotropic transformation strains imply that there must be a specific crystallographic orientation relationship between the α and β phases with respect to the phase transition.

Lastly, it is well established that transformation damage in the form of microcracks and voids is induced upon thermal cycling through the α–β transition. Furthermore, the size and number of cracks increases with continued α–β cycling, which leads to a volume expansion of the Pu metal specimens of as much as 3% (0.6 g/cm^3) per cycle [11]. A number of factors were found to influence the presence and pervasiveness of this transformation-induced damage, including how the parent β-phase was formed, concentration of impurities, transformation temperature, heating/cooling rates, and applied stresses.

The Pu β–γ phase transition has not been studied to the same extent as the α–β phase transition. It is known that the T–T–T curves for the γ–β phase transition have a shape similar to the isothermal reaction curves of the β–α transition [12]. A study on phase transformation damage in plutonium has shown that no physical damage occurs during γ–β cycling [11]. However, it was found that more physical damage (e.g., microcracking) occurs in α-Pu during the β–α phase transition if the β-Pu had been formed from α-Pu rather than γ-Pu. Thus, the thermal history can have a significant effect on damage accumulation and expansion during the β–α phase transition.

There are obviously a large number of variables which could influence how constrained pieces of α-Pu metal within a stainless steel storage container might behave when cycled through the α–β–γ phase transitions, and what effect the Pu metal may have on the integrity of the container. This illustrates the necessity for experimentally determining what effects the volume expansion associated with the α–β and β–γ phase transitions of plutonium metal may have on the integrity of such a container.

3. Experimental procedure

3.1. α–β experiment

The Pu source material used for these experiments was supplied by Westinghouse Savannah River Site, and consists of 10 year old high-purity alpha-phase metal in the form of ~2 kg buttons. The range of isotopic compositions and impurity concentrations in these buttons is given in Table 1. Based on the starting ^{241}Pu concentration and the age of the material, the total americium concentration was calculated to be approximately 1300–2000 wppm. The material was melted and chill cast at the plutonium foundry at Los Alamos National Laboratory (LANL) into a graphite mold, which resulted in an as-cast cylindrical ingot 11.45 cm in diameter and 1.98 cm in height, with a mass of 4231.3 g. Following casting, the ingot was machined to a right circular cylinder of the following dimensions: 11.069 cm diameter, 1.908 cm thickness, 3591.7 g mass. Using an immersion method, the density was measured to be 19.57 ± 0.01 g/cm^3. The high measured density (theoretical max. $\rho_{\alpha\text{-Pu}} = 19.86$ g/cm^3) and surface uniformity of the cast ingot indicated the absence of any significant microcracking or void space formation from the casting process. Previous studies indicate that the presence of certain impurities, such as Am, on the order of 1000 wppm, drastically reduce microcrack formation during casting [11]. Thus, the 1300–2000 wppm Am content of the material used in this study may in part be responsible

Table 1
Range of isotopic composition and impurity concentrations in the Pu source material

^{239}Pu	93.654–93.898
^{240}Pu	5.530–5.783
^{241}Pu	0.250–0.547
^{242}Pu	0.060
Si	<5–20
Ga	<2
Al	14–31
U	<25–36
Pu	<10
Cd	<2
Sn	<10
Cu	<1–44
Fe	105–151
Mn	5–14
Ni	<2–42
Zn	<5–8
Cr	<1–20
C	60–120
B	<4–18
Be	<0.1
Ca	<5–119
Mg	9–52

Isotopic compositions are in wt%, and impurity concentrations are in wppm.

for the observed high density and lack of significant microcracking.

In order to simplify subsequent finite element analyses of the experimental results, which were conducted by Westinghouse SRS [13–15], and eliminate any contribution to the wall strength of the container by a bottom or lid, an open-ended steel cylinder was used to simulate a DOE standard 3013 inner canister. Several of these cylinders were manufactured at Westinghouse SRS using 316 stainless steel via a process which resulted in a fully annealed product. The cylinder used for the α–β experiment was designated as SRS Part #3, and had dimensions reported by SRS as the following: 11.072 cm internal diameter (ID), 11.394 cm outer diameter (OD), 15.260 cm length, 1.52 mm thickness. The ID was re-measured upon arrival at LANL as 11.079 cm, which leaves a 0.050 mm radial clearance between the Pu ingot and ID of the cylinder.

Twelve strain gages were installed on the outer surface of the cylinder as per the manufacturer's (Micro-Measurements Division, Measurements Group, Raleigh, NC) instructions. Three types of strain gages were used. Eight small single direction gages (part EP-08-062-DN-350) were chosen to measure the hoop strain where the ingot is in contact with the cylinder. Two 5 cm long single direction gages (part EA-06-20CRW-120) were chosen to measure the axial strain across the entire thickness of the ingot, and a two-element 90° rosette was chosen to measure the axial and hoop strains in a region on the tube far from the ingot. A three-wire configuration was used to connect the gages to the recording equipment to prevent thermal drift due to resistance changes with temperature in the leads. Following installation, the continuity of the wiring was checked, and it was found that two of the hoop strain gages could not be used due to damage during installation. Input from these bad gages was subsequently ignored.

Three *K*-type thermocouples (Model SA1-K, Omega) were placed on the outside of the cylinder, and a fourth was placed on the Pu ingot itself. The thermocouples were attached via self-adhesive pads which are certified for use up to 160 °C. Prior to use, the thermocouples were calibrated in a controlled environment between 0–160 °C using equipment traceable to national standards by the LANL Standards and Calibration Laboratory, and certified to be accurate to ±0.3 °C. Output leads from the strain gages and thermocouples were connected to a National Instruments SCXI-1321Terminal Block. Strain and temperature data were recorded at 15 s intervals during the experiment via a custom written LabView software application.

For all thermal cycles, heating was done from ambient temperature to 130 °C at 2 °C/min in a Lindberg MK-6015-S, 208 V 4000 W horizontal open-ended tube furnace, 38.1 cm long, 15.2 cm ID with a custom built temperature controller. Cooling was done by turning off the furnace power and letting the experiment cool to ambient. All experiments took place within an Ar-atmosphere glovebox, with O_2 levels maintained at a concentration of 30 vppm or less.

Following installation of the furnace and steel cylinder into the glovebox, several strips of fiberglass cloth were laid down inside the bottom half of the tube furnace on which the cylinder was placed. This prevented direct contact of the outside of the cylinder, as well as the strain gages and thermocouples, with the heating elements of the furnace.

Thickness changes in the Pu ingot were measured using two quartz glass rod dilatometers attached to dial indicators (Part #196B, Starrett), accurate to ±0.025 mm. Readings from the dial indicators were recorded manually throughout the course of the experiments. A schematic of the entire experimental setup is given in Fig. 1.

Prior to performing the experiment using the Pu ingot, a 'dry run' was done in order to quantify the thermal response behavior of the strain gages installed on the stainless steel cylinder in the absence of any other strain. A brass ingot, of the same dimensions as the Pu ingot, was slid into the steel cylinder and centered by hand to act as a thermal mass. The cylinder and brass ingot were then thermally cycled in a manner identical to which the Pu ingot would be cycled (2 °C/min heating rate to 150 °C, 30–90 min at 150 °C, followed by power-off cooling to ambient temperature) and the response of

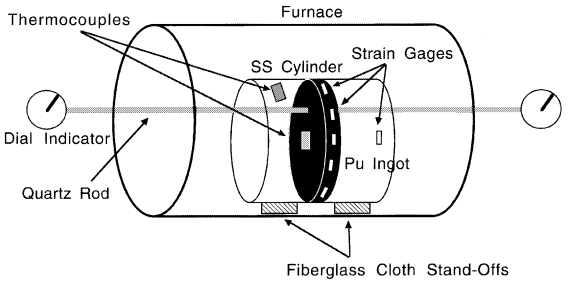

Fig. 1. Schematic of experimental setup (not to scale).

the strain gages recorded as a function of time and temperature. Note that no additional strains were applied to the cylinder by the brass ingot, which was used solely as a thermal mass. The far-field and axial strain gages showed a positive strain in response to temperature of 550 ± 20 microstrain ($\mu\varepsilon$) from ambient to 130 °C. The hoop strain gages showed negative strain in response to temperature of -250 ± 20 $\mu\varepsilon$ from ambient to 130 °C. These strains produced by the thermal response of the gages are small compared to the strains measured as a result of the Pu expansion. Thus, their contribution to the total strain measured was subsequently ignored.

Following the dry run, the brass ingot was removed from the cylinder and the Pu ingot was inserted by hand, a thermocouple was attached to the ingot, and the ingot was centered within cylinder with the aid of a ruler to within ± 1 mm. Quartz glass rod dilatometers were then placed on the opposing faces of the ingot and zeroed. All strain gages were zeroed prior to the first thermal cycle. This was the only time the strain gages were zeroed so that the cumulative effects of strain as a function of cycle could be measured.

3.2. α–β–γ experiment

The experimental procedure used for the α–β–γ experiment was similar to that used to examine the expansion associated with the α–β phase transition. The same Pu source material was used to chill cast and machine a second right circular cylindrical ingot of the following dimensions: 11.011 cm diameter, 1.857 cm thickness, 3470.9 g mass. Using an immersion method, the density was measured to be 19.62 ± 0.01 g/cm^3. The high measured density (theoretical max. $\rho_{\alpha-\mathrm{Pu}} = 19.86$ g/cm^3) and surface uniformity of the cast ingot indicated the absence of any significant microcracking or void space formation from the casting process. The stainless steel cylinder used for this experiment was designated as SRS Part #1, and had reported dimensions of: 11.072 cm internal diameter ID, 11.361 cm OD, 15.321 cm length, 1.4 mm thickness. The ID was remeasured upon arrival at LANL as 11.041 cm, which leaves a 0.15 mm radial clearance between the Pu ingot and ID of the cylinder.

Nine strain gages (part number: PHAE-125BA-350 LEN, JP Technologies) were installed on the outer surface of the cylinder as per the manufacturer's instructions. These gages were certified by the manufacturer for operation up to 250 °C. Their MicroMeasurements counterparts, which are made from the same materials and certified to only 205 °C, and the associated adhesive and installation procedure were examined in a separate experiment [16] and they were found to be reliable. Six gages were aligned to obtain hoop strain along the center line of the Pu ingot, two gages were aligned to obtain axial strain across the ingot, and one gage was placed in the far-field away from the region of anticipated strain.

Three *K*-type cement-on thermocouples (Model CO3-K, Omega) were placed on the outside of the cylinder. Two additional thermocouples were placed on the Pu ingot itself: one at the center of the ingot and one two-thirds of the radial distance between the center and edge of the ingot near the top of the cylinder. The thermocouples were affixed to the cylinder and Pu ingot using a high temperature high thermal conductivity epoxy rated to 260 °C (OmegaBond 200, Omega Engineering, Stamford, CT). During the course of the experiments, the thermocouples did not stay affixed to the Pu ingot due to expansion of the ingot through the phase transitions. In addition, some separation of the thermocouples from the steel cylinder was also observed due to the expansion of the cylinder. Teflon tape was found to adequately keep the thermocouples affixed to the cylinder, though there was still some difficulty in keeping the thermocouples affixed to the Pu ingot. Strain and temperature data were recorded at 15 s intervals.

The stainless steel cylinder was centered horizontally and vertically in the furnace tube using a custom built steel stand-off for vertical centering. For the first three thermal cycles, heating was done from ambient temperature to 250 °C in an hour and a half (~2.5 °C/min). The fourth cycle was done from 102 °C (beta phase) to 260 °C in one hour (~2.6 °C/min). Cooling was done by turning off the furnace power and letting the experiment cool to ambient. All experiments took place within an Ar-atmosphere glove box, with O_2 levels maintained at 500 vppm or less.

3.3. Metallography

Optical metallographic analyses of Pu metal samples cut from the ingots were conducted using LECO 300 and Leicia DMIRM metallographs. Metal samples were cut from the ingots and vacuum mounted in epoxy holders. The surface to be observed was mechanically

polished using 1 μm diamond grit and then electropolished.

4. Results

4.1. α–β experiment

The strain and temperature vs. time data from the first cycle are given in Fig. 2. All of the hoop strain gages showed peak positive strains ranging from 1.04% to 1.75% during the course of the thermal cycle. In contrast, the axial gages showed a negative strain of −0.24%. The far-field gages showed only the expected thermal response of the empty cylinder, indicating no additional strain was accumulated away from the area in which the ingot was in contact with the cylinder. (Note that the temperature plotted in Fig. 2 is the temperature of the Pu ingot. Thus, the starting temperature of 52 °C is due to self-heating effects.) A plot of strain as a function of ingot temperature during the heating phase of the cycle is given in Fig. 3. Based on this first cycle, the calculated total strain on the steel cylinder averaged among all hoop strain gages is 1.44%. As is evident from Fig. 2, a large proportion of this strain is plastic (1.27% average), given that only a small amount of strain relaxation is observed after cooling. Subtracting the plastic from the total strain leaves the elastic strain, which is 0.17% on average for the first cycle.

Using the output from the hoop strain gage which consistently showed the highest strain, a plot of strain vs. time for all six cycles is given in Fig. 4. Six regimes of the strain vs. time plot for the first cycle are identified and interpreted as follows: (1) the first regime labeled represents strain accumulated due to the thermal expansion of α-Pu. Prior to this point, the flat part of the curve represents the time before the furnace was turned on, and the small amount of expansion of the α-Pu needed to close the 0.05 mm radial gap between the ingot and inside of the cylinder. (2) At approximately 120 min, the slope of the strain vs. time curve increases, and the second region represents strain accumulation due to expansion associated with the α to β phase transition. The thermal energy input is partly consumed by the endothermic α to β phase transition, and thus the temperature does not increase significantly during this time, as can be seen in Fig. 2, which is the characteristic of first-order phase transitions. (3) The strain peaks at the end of the phase transition, and then decreases slightly as the temperature is held constant. This strain decrease is most likely due to creep of the β-phase under the load imposed by the walls of the cylinder. (4) Once the furnace is turned off, a slight decrease in strain is observed due to load reduction from thermal contraction of the β-phase, followed by (5) a small but sharp drop in strain due to the β to α phase transition. Note that during the β to α phase transition, the temperature of the Pu ingot also increases slightly due to the release of the latent heat of the exothermic β to α phase transition (see Fig. 2). (6) Following the β–α phase transition, no further

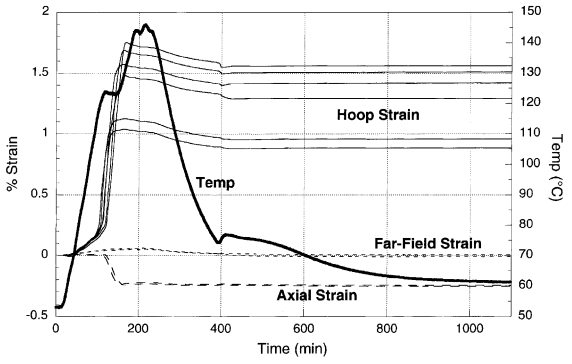

Fig. 2. Strain and temperature vs. time for first thermal cycle through α–β phase transition.

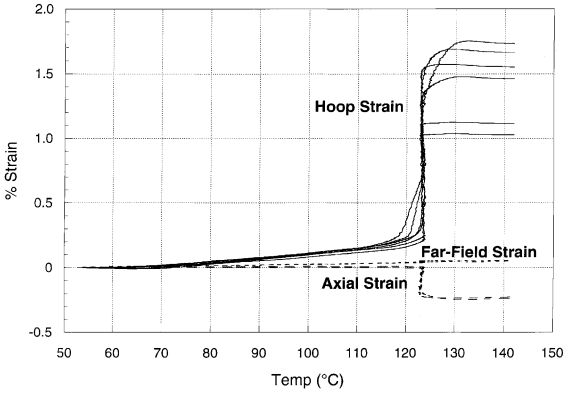

Fig. 3. Strain vs. temperature for first thermal cycle through α–β phase transition.

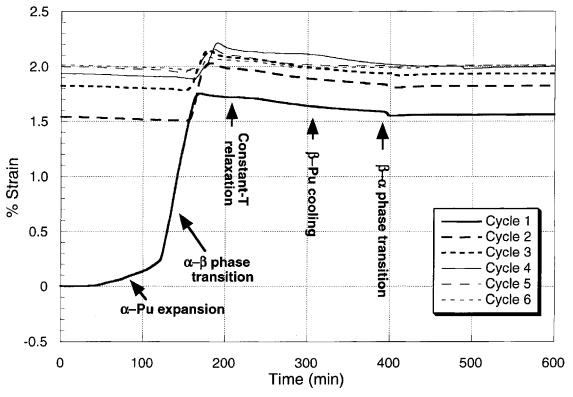

Fig. 4. Hoop strain vs. time for highest measured strain for all α–β cycles.

reduction in the strain was measured indicating that the cylinder was plastically deformed during this cycle.

As is evident from Fig. 4, most plastic strain in the cylinder is accumulated during the first thermal cycle. With each subsequent cycle, the amount of additional accumulated plastic strain decreases until cycle 6, in which no additional plastic strain is observed. A plot of the average total, plastic, and elastic hoop strain accumulated within each cycle is given in Fig. 5. The total plastic strain in the cylinder observed for all cycles, obtained by summing the plastic strain accumulated during each cycle, is 1.47% averaged over all hoop strain gages, and the maximum strain is 2.03%.

Dilatometry data is presented for the first and fourth cycle in Figs. 6 and 7, respectively. The change in thickness of the ingot was calculated by adding the measurements from the two opposing dilatometers. In Fig. 6, both the change in thickness of the ingot and the hoop strain from the gage showing the highest strain are plotted as a function of temperature. A small increase in thickness (0.025 mm, 0.13%) was observed prior to the onset of the phase transition, which is consistent within

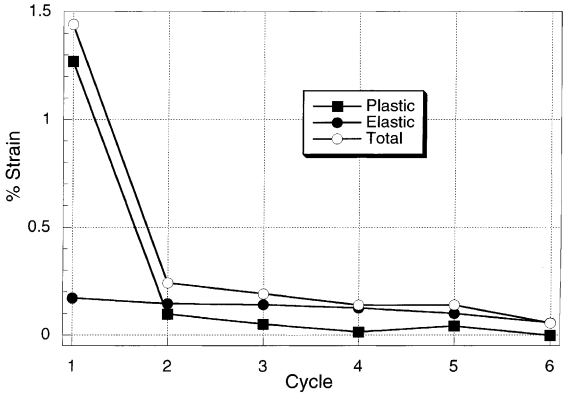

Fig. 5. Average strain vs. cycle for α–β experiment.

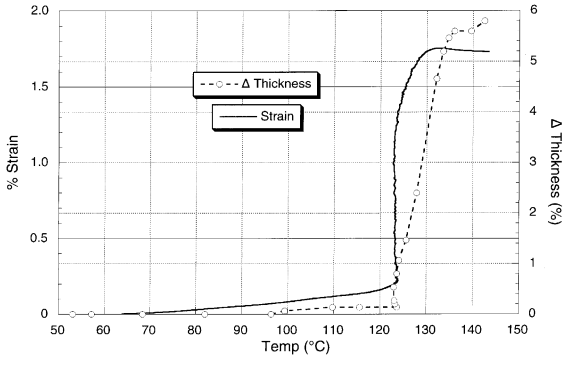

Fig. 6. Strain and change in thickness vs. temperature for first cycle through α–β phase transition.

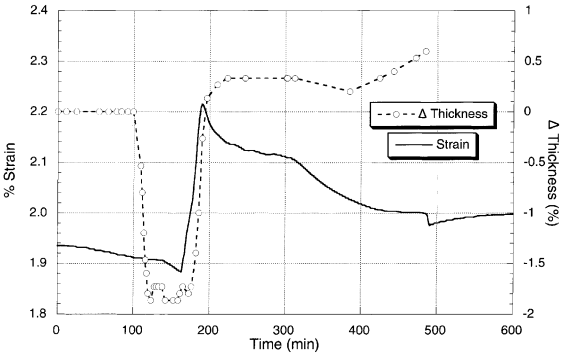

Fig. 7. Strain and change in thickness vs. temperature for fourth cycle through α–β phase transition.

error with the linear thermal expansion expected for α-Pu (~0.5%) over the temperature range from ambient to 110 °C [17]. Starting at the onset of the phase transition, as indicated by the sharp increase in strain, the thickness increased by 1.07 mm (5.8%) during heating. This is nearly twice the expected linear thermal expansion (~3%) for the unconstrained volume expansion associated with the α to β phase transition.

In Fig. 7, hoop strain and the thickness change are plotted as a function of time for the fourth cycle. Prior to the onset of the phase transition, a marked *decrease* in thickness (−1.8%) was observed, followed by a modest thickening of the ingot of 0.6% (over the starting thickness) during and after the phase transition.

Following the sixth thermal cycle, the ingot was removed from the cylinder and the cylinder OD at the midpoint was measured and found to have increased by 1.80 mm. Based on an initial OD of 11.372 cm, this represents a 1.58% increase in circumference, in good agreement with the measured strain of 1.32% averaged over all hoop gages. The plastic deformation of the cylinder was visible as a slight bulge around the waist. Despite the low oxygen levels generally maintained in the glovebox (<30 vppm), the Pu ingot showed surface oxidation upon removal from the cylinder. This oxidation may have been a result of above ambient temperatures, and thus higher reactivity, or due to a single overnight loss of negativity in the glovebox which resulted in significantly higher O_2 levels. Despite the coating of oxide, the ingot was still intact as a single massive piece of metal following the experiment with no obvious signs of cracking. The density of the ingot after six thermal cycles was measured to be 19.38± 0.01 g/cm^3, representing a 0.97% decrease from the as-cast density of 19.57 g/cm^3.

Reflected light metallographic photomicrographs from as-cast α-Pu metal and from the ingot cycled through the α–β phase transition are shown in Figs. 8 and 9, respectively. Metallography of the as-cast α-Pu

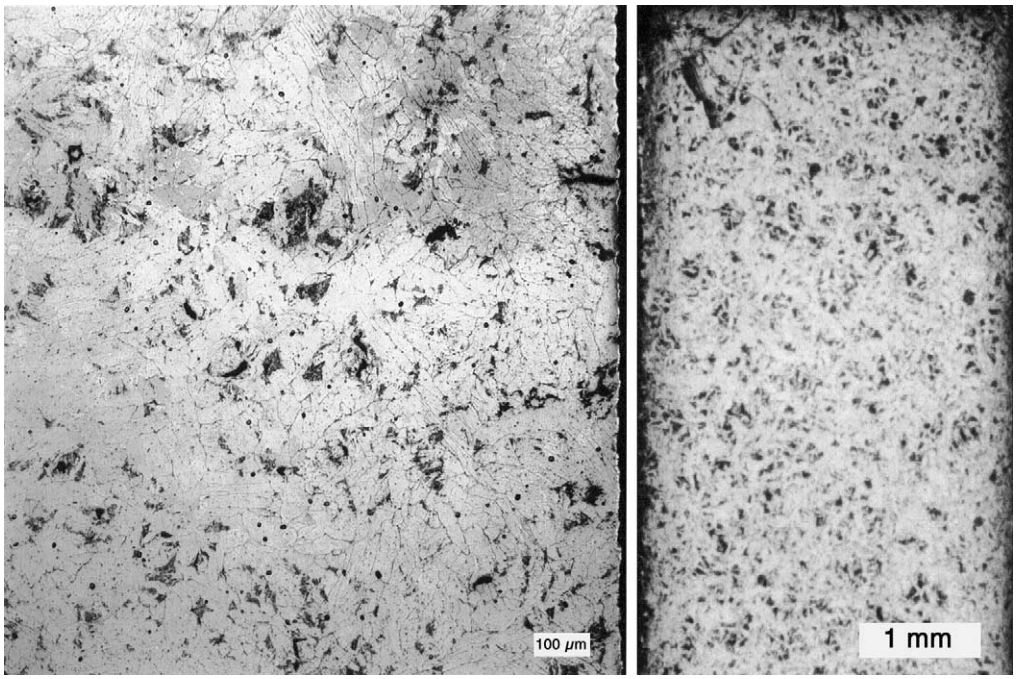

Fig. 8. Metallographic photomicrographs of as-cast α-Pu. *Left image* shows top surface of cylindrical ingot (axial view), *Right image* shows cross-section through ingot.

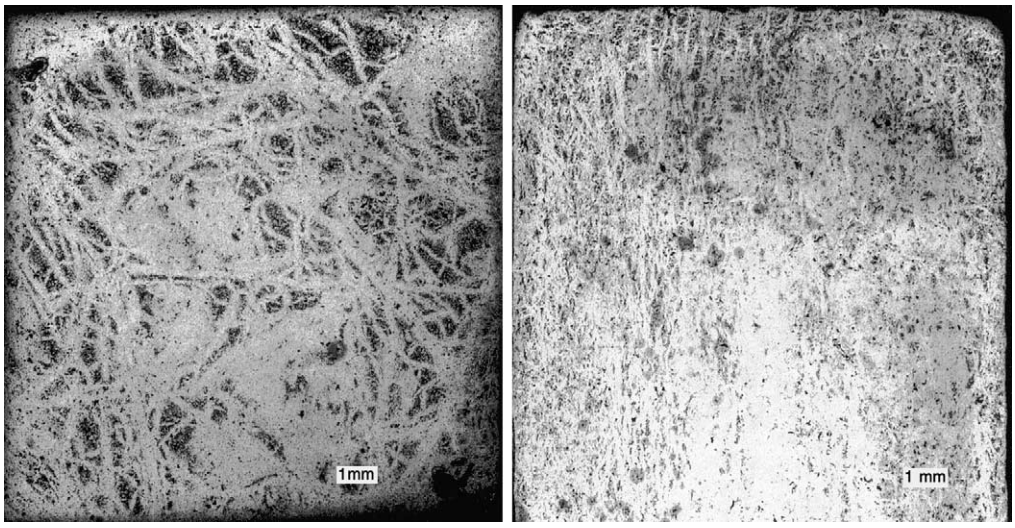

Fig. 9. Metallographic photomicrographs of Pu ingot cycled through the α–β phase transition. *Left image* shows top surface of cylindrical ingot (axial view), *Right image* shows cross-section through ingot.

(Fig. 8) shows a veined texture on the millimeter scale (right image in Fig. 8), which is characteristic of Pu metal that has cooled through the β–α phase transition [9]. These veins are made of up stacked disks of α-Pu with their (020) planes aligned perpendicular to the direction of compressive stress. This veining is random in its orientation in all metallographic images taken of as-cast ingot (both in cross section and axial views), thus indicating an absence of any compressive stress during the casting. On a 100 μm scale (left image in 8), individual euhedral grains of α-Pu are clearly visible, and show no preferential orientation.

After being cycled through the α–β phase transition, the veining texture becomes more pronounced, with longer and wider veins, as is evident in Fig. 9. Along the axial direction of the ingot, the veins are random in orientation (left image in Fig. 9). However, in cross section (perpendicular to the strain direction), the veins are aligned perpendicular to the stress direction imposed by the can (parallel to the axial direction of the ingot).

4.2. α–β–γ experiment

The strain and temperature vs. time data for the first α–β–γ cycle is given in Fig. 10. All of the hoop strain gages showed peak positive strains for all cycles, as did the axial gages. The far-field gage showed only the expected thermal response of an empty cylinder, indicating no plastic strain was accumulated away from the area in which the ingot was in contact with the cylinder. Due to the larger radial clearance between the machined ingot and the ID of the cylinder in this experiment (0.15 mm) relative to the α–β experiment (0.05 mm), contact between the ingot and the cylinder wall is observed just prior to the onset of the α–β phase transition (~110 °C) in this experiment rather than 40 °C below the transition temperature (~70 °C) as in the previous experiment. Based on the mean linear thermal expansion coefficient of 53.8×10^{-6} /°C for α-Pu [17], and the difference in the radial clearances between the previous and current experiments, a 34 °C difference in the temperature at which the ingot makes contact with the wall in the previous and current experiments is expected. This is consistent with the ~40 °C difference observed.

Using the output from the hoop strain gage that consistently showed the highest strain, a plot of strain vs. time for all four cycles is given in Fig. 11. (The data from cycles 2 and 3 have been offset along the x-axis so that the onset of the β–γ transition occurs at the same time as observed in the first cycle.) During the first cycle, the onset of the β–γ transition is apparent as an accumulation of additional strain between 180 and 200 min. Following the β–γ transition, there is a slight decrease in strain at constant temperature, presumably due to creep of the γ-phase under the restraint imposed by the walls of the cylinder. Upon cooling, a linear decrease in strain was observed for all hoop and axial gages consistent with the thermal contraction of γ-Pu, followed by an abrupt decrease in strain due to the onset of the γ–β back transformation. All strain values are constant throughout the remainder of the cooling part of the cycle, indicating that accumulated plastic strain was greater than total strain imparted by the α–β transition (i.e., there is no evidence of the β–α back transformation in the strain data).

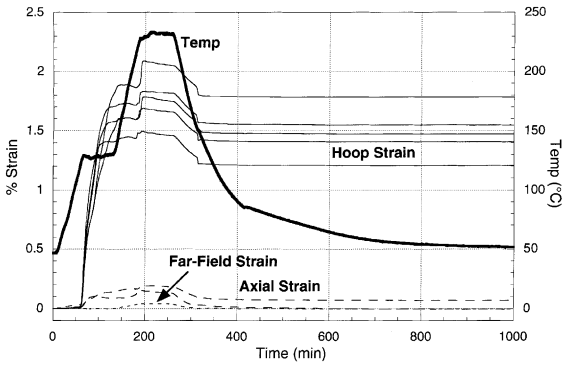

Fig. 10. Strain and temperature vs. time for first thermal cycle though α–β–γ phase transitions.

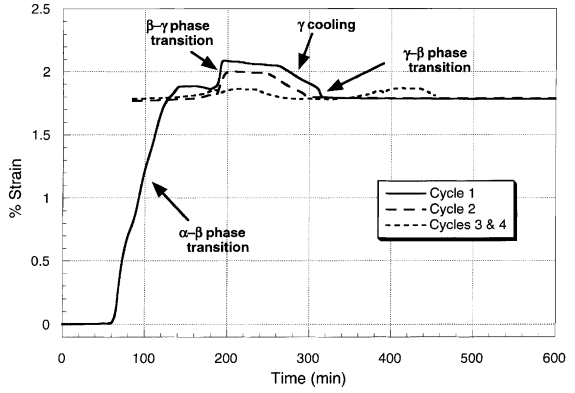

Fig. 11. Hoop strain vs. time for highest measured strain for all α–β–γ cycles.

During the second thermal cycle there is no evidence of the α–β transition in the strain data, which is consistent with the observations during cooling from the first cycle, suggesting that the accumulated plastic strain in the wall is greater than the total strain imparted by the α–β transition of the Pu. The β–γ phase transition of the Pu is again evident as an increase in wall strain at a temperature above 220 °C, and a linear decrease in wall strain is observed upon cooling, which is consistent with the first cycle.

During the third and fourth heating cycles, the ingot was brought up through the α–β and β–γ phase transitions, cooled through the γ–β back transformation, reheated through the β–γ transition, and then allowed to cool to ambient temperature. This was done to determine if cycling through only the β–γ phase transition would affect the accumulated strain in a manner different from the α–β–γ–β–α progression used in the first two cycles. A plot of the average total, plastic, and elastic hoop strain accumulated within each cycle is given in Fig. 12. The total amount of plastic strain in the wall observed for all cycles, obtained by summing the amount of plastic strain accumulated during each cycle, is 1.55% averaged over all hoop strain gages, and the maximum strain is 1.79%.

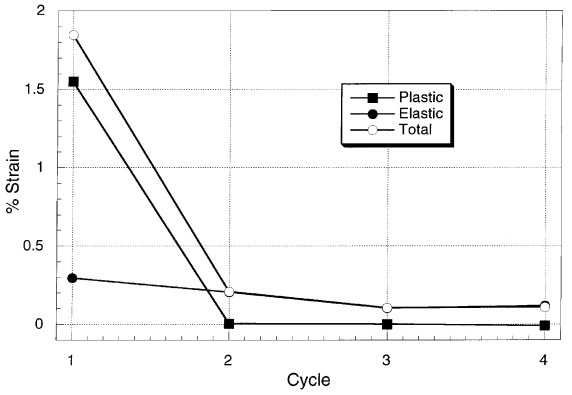

Fig. 12. Average strain vs. cycle for α–β–γ experiment.

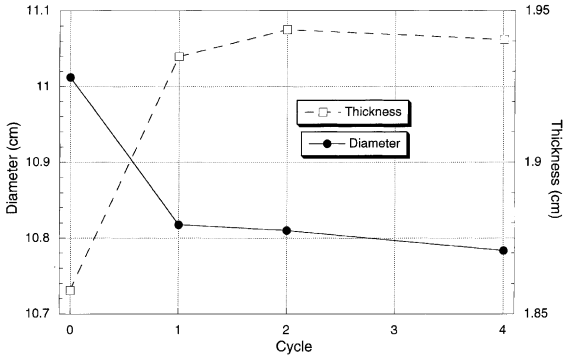

Fig. 13. Ingot diameter and thickness vs. cycle for α–β–γ experiment.

Dilatometry was not used during the α–β–γ experiment. Rather, following each cycle the Pu ingot was removed from the cylinder and the thickness and diameter were measured to evaluate any changes in shape or volume as a result of the stress imposed during the phase transitions. The results are plotted in Fig. 13. Following the first cycle, the diameter of the ingot decreased by 1.8% (−1.95 mm) and the thickness increased by 4.2% (0.77 mm) relative to the as-machined ingot, resulting in a volume change of +0.5%. Following the second and fourth cycles, the diameter of the ingot continued to decrease slightly (0.3% total, 0.34 mm), while the thickness remained nearly constant. After the first cycle, the surface of the ingot also took on a more textured appearance relative to the freshly machined surface. The density of the ingot at the end of the experiment was measured to be 19.57 ± 0.01 g/cm^3, which is only 0.25% less than the as-cast density of 19.62 g/cm^3.

Reflected light metallographic photomicrographs from the ingot cycled through the α–β–γ phase transitions are shown in Fig. 14. Note the coarse veining texture similar to the as-cast material in Fig. 8, and the lack of any preferred orientation to the veins as observed in Fig. 9.

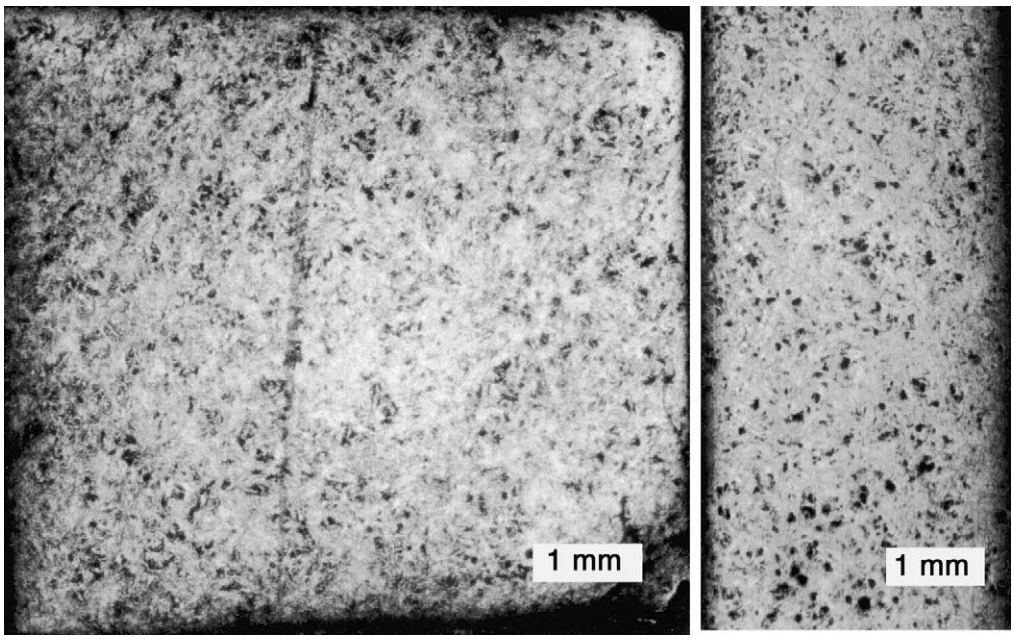

Fig. 14. Metallographic photomicrographs of Pu ingot cycled through the α–β–γ phase transitions. *Left image* shows top surface of cylindrical ingot (axial view), *Right image* shows cross-section through ingot.

5. Discussion

5.1. α–β experiment

Overall response of the strain gages during thermal cycling is as expected for expansion and contraction of the Pu ingot within the stainless steel cylinder. The hoop strain gages all showed positive strains, while the axial gages showed a slight negative strain, corresponding to compression, which is consistent with radial expansion of the cylinder. We can estimate the elastic hoop strain using Hooke's Law:

$$\varepsilon_\theta = \frac{1}{E}[\sigma_\theta - \nu(\sigma_r + \sigma_z)] + \alpha(T - T_0), \tag{1}$$

where ε_θ is elastic hoop strain, σ is stress in the 3 principle directions (note that $\sigma_r = 0$), E is elastic modulus, ν is Poisson's ratio, α is expansion coefficient, T is temperature at maximum strain, and T_0 is temperature at strain relaxation. To approximate the highest loading on the Pu, the wall stress can be set equal to the tensile yield strength of the stainless steel, measured as 280 MPa at the SRS. Using values of $E = 188{,}280$ MPa (measured by SRS for the steel cylinder), $\alpha = 1.73 \times 10^{-5}$ /°C, $\nu = 0.27$ (typical values for 300-series stainless steel), $T = 124$ °C, and $T_0 = 62$ °C, and making the assumption that $\sigma_\theta = \sigma_z$, the elastic strain calculated is 0.00215, which compares favorably with the measured value of 0.00171 from the first cycle.

Based on the geometry of thin-walled cylinders [18], the radial compressive stresses experienced by the Pu ingot during the phase transition can be estimated based on the following relationship:

$$\sigma_\theta = \frac{Pr}{t}, \tag{2}$$

where σ_θ is hoop stress, P is internal pressure, r is radius of cylinder, and t is wall thickness. As a simple approximation, the wall stress can be set equal to the tension yield strength of stainless steel. Using the appropriate dimensions of the cylinder ($r = 5.540$ cm, $t = 1.52$ mm), the calculated internal pressure, equivalent to the compressive stress applied to the Pu ingot, as a result of the expansion is 7.70 MPa. The calculated value would be increased by about 10% if the plastic deformation were included. However, this approximation ignores the axial deformation and the temperature effect, both of which would decrease the stress.

The calculated radial compressive stress imparted on the Pu ingot by the cylinder wall is far less than the compressive yield strength values of both α-Pu (~410 MPa) and β-Pu (~140 MPa) at the transition temperature [17]. Therefore, the axial deformation observed in the Pu ingot must be due to some mechanism other than simple compressive yield. This is consistent with previous observations that stresses applied during either the α to β or β to α phase transitions produce pronounced crystallographic and microstructural shape texturing [8,10]. The 'veining phenomenon' observed in the metallographic images of the as-cast and cycled ingots confirm this. The dilatometry data presented in Fig. 6 suggest that during the α–β phase transition, a preferential grain alignment is established perpendicular to the radial stresses imposed by the walls of the cylinder, resulting in a thickening of the ingot greater than would be expected based on isotropic expansion. The greatest amount of strain would therefore be placed on the Pu ingot during the first cycle when the grain orientation is random. Additional strain from subsequent cycles would be substantially less due to the preferred grain alignment perpendicular to the stress direction and accompanying preferred expansion in the axial direction, which is exactly what is observed in the experimental strain data.

The equilibrium temperature for the α to β phase transition is 120 °C [7]. However, in all cycles the observed onset of the α to β phase transition was around 123 °C and the onset of the β to α back transformation was around 75 °C. These values are consistent with the known T–T–T behavior of Pu [12,19]. The α–β start time is quite long (>1000 s) at temperatures below about 120 °C. At 140 °C, the maximum temperature that the ingot reached during the thermal cycling, the α to β completion time is of the order of 10^3 s, which is consistent with what was observed. For the β to α back transformation, the T–T–T curves show that the transformation times do not reach values of less than 10^3 s until the temperature is less than about 80 °C, which is also consistent with what was observed experimentally.

The increase in ingot thickness though the phase transition for the first cycle, as depicted in Fig. 6, is expected. As mentioned above, the increase in thickness beyond the amount anticipated for isotropic expansion is due to preferential grain alignment during recrystallization as a result of the imposed stresses from the cylinder wall. The decrease in ingot thickness observed immediately prior to the α to β phase transition (Fig. 7) for all cycles following the first could be the result of two different factors. One possibility is that some β-Pu is retained upon cooling from the previous cycle. During the heating phase of the next cycle, this quenched β-Pu recrystallizes prior to the phase transition. However, this seems an unlikely possibility as the β to α T–T–T curves show that the β to α transformation is most efficient between −40 and +40 °C [19]. Even at 50 °C (the equilibrium temperature of the Pu ingot in this experiment), the transition begins in <10 s, and is 5% complete in only 12 s. A more likely explanation of the contraction of the ingot immediately prior to the α to β phase transition is annealing of microcracks formed in the α-Pu as a result of the previous β to α transformation. As has been previously reported [11], the volume expansion

associated with cycling Pu across the α–β phase transition is due to the formation of microcracks, and the 0.97% decrease in density of the ingot following the α–β experiment suggests some microcracking has occurred. The microcracks can be annealed out by heating α-Pu to within 10–20 °C of the transition temperature [20]. Thus, it seems more likely that the contraction observed prior to the onset of the phase transition is due to the annealing of microcracks within α-Pu than recrystallization of residual β-Pu back to α-Pu. Regardless of the mechanism, the observed contraction appears to have little effect on the overall integrity or deformation of the cylinder.

It is readily apparent from Figs. 2 and 3 that not all strain gages showed response to the phase transition at exactly the same time (or temperature, relative to the ingot temperature), nor do they show the same values of total strain. This result may in part be due to non-uniform expansion of the ingot or slight asymmetry in the roundness of the cylinder or ingot causing the ingot to come in contact with different parts of the cylinder wall at different times. Another possible explanation is differential heating effects and temperature inhomogeneity.

5.2. α–β–γ experiment

As is evident from Fig. 12, all of the plastic strain (1.55%) was accumulated during the first cycle. No additional plastic strain was observed in the following cycles. The elastic strain observed during the first cycle was 0.30%, which decreased to 0.20% in the second cycle, and leveled out at 0.10% in the third and fourth cycles. This is substantially different from what was observed during the α–β experiment, in which additional plastic strain was accumulated through five cycles of the α–β transition. As would be expected, the average peak strain (plastic and elastic) during the first cycle for this experiment (1.85%) is greater than for the previous α–β experiment (1.44%). However, the average total accumulated plastic strain for this experiment (1.55%) is very close to that observed for the previous α–β experiment (1.47%).

A plot of the total strain per cycle and cumulative plastic strain for both the α–β and α–β–γ experiments is shown in Fig. 15. As mentioned above, the total amount of plastic strain imparted upon the canister by the ingot is nearly the same for both experiments (1.47% for the α–β expansion vs 1.55% for the α–β–γ expansion). However, as is evident from Fig. 15, the manner in which the plastic strain is accumulated is different between the α–β and α–β–γ experiments. In the first (α–β) experiment, the total amount of plastic strain is accumulated over the first four cycles. In contrast, in the second (α–β–γ) experiment, all of the plastic strain is accumulated in the first cycle, with no additional plastic strain imparted during subsequent cycles.

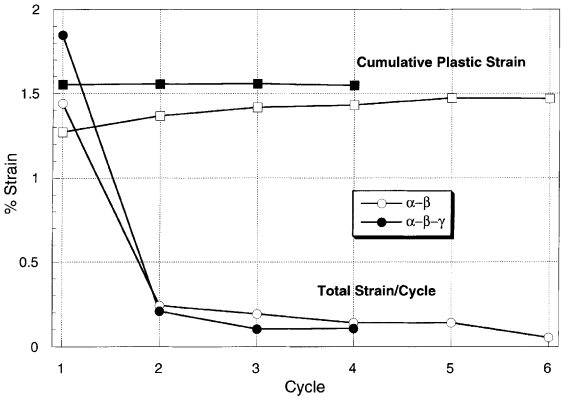

Fig. 15. Total average strain per cycle and cumulative plastic strain vs. cycle for both the α–β (open symbols) and α–β–γ (filled symbols) experiments.

In the α–β experiment, the ingot does not disengage from the cylinder upon cooling until after the β–α back transformation initiates (Fig. 4), and in subsequent cycles the ingot re-engages the cylinder upon heating prior to the completion of the α–β transition. In contrast, in the α–β–γ experiment, the ingot disengages from the cylinder at the beginning of the γ–β back transformation (Fig. 11), and in subsequent cycles the ingot does not re-engage the cylinder until the β–γ transition. Thus, in the α–β–γ experiment, all of the plastic deformation to the cylinder is done during the first cycle when it is in contact with the ingot during the expansion of both the α–β and the β–γ phase transitions. In all successive cycles, the cylinder is only in contact with the ingot during the β–γ expansion, which only elastically strains the cylinder.

As evident from Fig. 13, the ingot was also deformed after the first cycle, becoming thicker and smaller in diameter. This, in part, explains why there is no additional plastic deformation to the cylinder after the first cycle, and why the ingot does not re-engage the cylinder until the onset of the β–γ transition on subsequent cycles: due to its smaller diameter it must expand further in order to re-engage the cylinder. From a microstructural standpoint, it is not immediately obvious as to why the ingot in the α–β–γ experiment should be deformed so. Metallographic images from the α–β experiment (Fig. 9) show an oriented veining texture that had previously been determined to be a result of α-Pu grains oriented perpendicular to stress imposed during the α–β transformation. However, metallographic images of the ingot from the α–β–γ experiment (Fig. 14) do not show the oriented veining texture as seen in Fig. 14, and instead appear very similar to the as-cast ingot (Fig. 8). Anisotropic deformation to the ingot must have occurred during the α–β and/or β–γ transitions upon heating when the ingot was in contact with the cylinder wall and

under stress. Any preferential grain orientation as a result of this could have then been overprinted during the subsequent stress-free transformations, resulting in the texture observed in Fig. 14. In addition, the small change in density of the ingot (−0.25%) relative to the as-cast material suggests that cycling through the α–β–γ phase transitions results in metal with a low concentration of microcracks, similar to as-cast material.

6. Conclusion

The highest level of total plastic strain that was imparted on the stainless steel cylinder by the Pu ingot during the α–β experiment was 2.03%. If the ~0.2% elastic strain is added to this, then the total amount of strain (plastic plus elastic) experienced by the cylinder was ~2.2%. The average total plastic strain, based on all hoop strain gages, is only 1.47%. These strain levels are far below the plastic failure strain levels for this type of stainless steel. Using the measured elastic strain values, the maximum radial compressive stress that the cylinder could impart upon the Pu ingot is about 8.96 MPa. The result of this compressive stress is that expansion of the ingot in the axial direction was measured to be greater than 5%, which is well above the 3% expected for isotropic expansion. This enhanced axial expansion is due to preferential grain orientation ('veining phenomenon') along the axial direction due to the radial stress imposed on the ingot by the can while expanding through the α–β phase transition.

Repeated thermal cycling of the ingot resulted in a decrease in the amount of additional plastic strain accumulated within each cycle, such that by cycle 6 no additional plastic strain was imparted upon the cylinder. This decrease is attributed to the preferential orientation of grain growth during the multiple α–β phase transitions, thereby limiting the expansion in the radial direction.

The highest level of plastic strain that was imparted on the stainless steel cylinder by the Pu ingot upon cycling through the α–β–γ phase transitions was 1.78%. If the ~0.2% elastic strain is added to this, then the total amount of strain (plastic plus elastic) experienced by the cylinder was ~2.0%. However, the average total plastic strain, based on all hoop strain gages, is only 1.56%. As with the α–β experiment, these strain levels are far below the plastic failure strain levels for this type of stainless steel.

Repeated thermal cycling of the ingot through the α–β–γ phase transitions resulted in no additional increase in the amount of plastic strain accumulated within each cycle. Following the first cycle, the Pu ingot was observed to have decreased in diameter by 1.8% and the thickness increased by 4.2% relative to the as-machined ingot, resulting in a volume change of +0.5%. Unlike the ingot from the α–β experiment, metallographic images of the ingot from the α–β–γ experiment do not show the oriented veining texture, which would be indicative of applied stress during the α–β transformation. Instead, the texture appears very similar to the as-cast ingot. The deformation to the ingot occurred either during the α–β and/or β–γ transitions upon heating when the ingot was in contact with the cylinder wall and under stress. Any preferential grain orientation as a result of this was thus overprinted during the subsequent stress-free transformations.

In-depth analysis of these results using Finite Element Analysis and a comparison with ASME code has been performed by Westinghouse Savannah River [15]. This study concluded that there is no credible threat to the integrity of the stainless steel storage containers from the expansion of Pu up through the β–γ phase transition.

Acknowledgements

The authors would like to thank the following people for their invaluable contributions to this study: John Y. Huang and Kenny M. Vigil for the plutonium casting, Anthony F. Valdez for the density measurements, Steven L. Boggs and Charles T. Owens for the plutonium machining operations, and Fredrick G. Hampel and Paul E. Danielson for the metallographic imaging. We would also like to thank Arthur 'Lonny' Morgan and Ann Schake for their invaluable assistance in setting up and conducting this study. This work was supported by the Nuclear Materials Stewardship Project Office of the United States Department of Energy.

References

[1] DOE, DOE-STD-3013-96, US Department of Energy, 1996.
[2] ASME, Section VIII, Division 2, Boiler and Pressure Vessel Code, American Society of Mechanical Engineers, 1995.
[3] DOE, DOE-STD-3013-99, US Department of Energy, 1999.
[4] R.D. Nelson, J.C. Shyne, J. Nucl. Mater. 19 (1966) 345.
[5] R.D. Nelson, J.C. Shyne, Trans. Metall. Soc. AIME 236 (1966) 1725.
[6] J.J. Rechtien, R.D. Nelson, Metall. Trans. 4 (1973) 2755.
[7] D.R. Stephens, J. Phys. Chem. Solids 24 (1963) 1197.
[8] B. Spriet, Study of allotropic transformation of plutonium, in: Plutonium 1965, Chapman and Hall (The Institute of Metals), London, 1965.
[9] J.S. White, J. Nucl. Mater. 59 (1976) 77.
[10] R.O. Elliot, C.E. Olsen, S.E. Bronisz, Phys. Rev. Lett. 12 (1964) 276.

[11] R.D. Nelson, J. Nucl. Mater. 20 (1966) 153.
[12] R.D. Nelson, Solid state reactions, in: O.J. Wick (Ed.), Plutonium Handbook, vol. I & II, American Nuclear Society, La Grange Park, IL, 1980, p. 101.
[13] H.E. Flanders, T-CLC-G-00113, Westinghouse Savannah River Company, 1999.
[14] H. Flanders, T-CLC-G-00127, Westinghouse Savannah River Company, 1999.
[15] H. Flanders, T-CLC-G-00125, Westinghouse Savannah River Company, 1999.
[16] D.K. Veirs, H. Flanders, D. Spearing, C. Prenger, LA-UR-99-5370, Los Alamos National Laboratory, 1999.
[17] W.N. Miner, F.W. Schonfeld, Physical properties, in: O.J. Wick (Ed.), Plutonium Handbook, vol. I & II, American Nuclear Society, La Grange Park, IL, 1980, p. 31.
[18] E.P. Popov, Mechanics of Materials, Prentice-Hall, Englewood Cliffs, NJ, 1976.
[19] R.D. Nelson, J. Nucl. Mater. 23 (1967) 238.
[20] J. Huang, T. Jenkins, Los Alamos National Laboratory, 1998, personal communication.